Journal of Alloys and Compounds 509 (2011) 6585–6588

Contents lists available at ScienceDirect

Journal of Alloys and Compounds

journal homepage: www.elsevier.com/locate/jallcom

Enhanced visible-light-response photocatalytic activity of bismuth ferrite nanoparticles

Xiong Wang*, Ying Lin, Xifeng Ding, Jinguo Jiang

School of Materials Science and Engineering, Nanjing University of Science and Technology, Nanjing 210094, China

ARTICLE INFO

Article history:
Received 15 December 2010
Received in revised form 1 March 2011
Accepted 11 March 2011
Available online 25 March 2011

Keywords:
$BiFeO_3$
Nanomaterials
Visible light irradiation
Photocatalytic

ABSTRACT

Multiferroic $BiFeO_3$ nanoparticles were prepared by a sol–gel rapid calcination technique with average diameter of 35 nm with narrow size distribution. The band gap was determined to be 2.06 eV, indicating their potential application as visible-light-response photocatalyst. The photocatalytic behaviors of $BiFeO_3$ nanoparticles were estimated by the degradation of Rhodamine B (RhB) under visible light irradiation. And the photocatalytic activities under different pH values were further studied for the first time. The result shows that the $BiFeO_3$ nanoparticles exhibit the highest photocatalytic activity in the solution with the lowest pH value, almost 100 times higher than that of the bulk.

1. Introduction

$BiFeO_3$, as one of the multiferroic materials, posseses ferroelectric and magnetic order at the same time. Therefore, it's been widely used in magnetic and ferroelectric devices [1,2]. $BiFeO_3$ has been fabricated by traditional solid state route which needs high temperature and subsequent acid washing [3,4]. Some soft-chemical methods such as hydrothermal [5–7] and sol–gel method [8–10] were developed to realize the uniform mixing of raw materials and to reduce reaction temperature. But some impurities like $Bi_{36}Fe_{24}O_{57}$ and $Bi_2Fe_4O_9$ exited unavoidably in the sample fabricated by a sol–gel method with $Bi(NO_3)_3{\cdot}5H_2O$ and $Fe(NO_3)_3{\cdot}9H_2O$ dissolved in 2-methoxyethanol and annealed at 600 °C for 30 min [11]. Another phase $Bi_{25}FeO_{40}$ still appeared in the powders synthesized by hydrothermal route [6]. Thus, preparation of pure phase $BiFeO_3$ is still a great challenge.

Recently, it was found that many materials such as $LaMnO_3$ and $LaCoO_3$ [12] with Perovskite structure like $BiFeO_3$ have attracted great interest in photocatalysis field. Recently, Liu and co-workers first studied the photocatalytic activity of $BiFeO_3$ nanoparticles in MO (methyl orange) solution [13]. In this paper, the pure phase $BiFeO_3$ nanoparticles were successfully prepared by a sol–gel rapid calcination technique, and meanwhile, considerable work was done to research the visible-light-induced photocatalytic property of $BiFeO_3$ nanoparticles under different pH values. Furthermore, the room-temperature weak ferromagnetism of $BiFeO_3$ will facilitate the separation of the catalyst from the aqueous solution. All those endow potential fascination to $BiFeO_3$ nanostructures for the promising application in water treatment.

2. Experimental

2.1. Preparation

The $BiFeO_3$ nanoparticles were synthesized by a sol–gel rapid calcination technique. All the reagents were analytical reagent grade and were used as received without further purification.

In a typical synthesis, 15 mmol bismuth nitrate pentahydrate ($Bi(NO_3)_3{\cdot}5H_2O$) was first dissolved in 36 mL ethylene glycol (EG, $HOCH_2CH_2OH$) to form a transparent solution. Then 15 mmol ferric nitrate nonahydrate ($Fe(NO_3)_3{\cdot}9H_2O$) was added into the solution. After magnetic stirring for 1 h, a brownish red colloidal sol was obtained. The solution was dried at 80 °C for 48 h and the $BiFeO_3$ xerogel powder formed. The xerogel was preheated at 400 °C for 0.5 h to remove organic compounds and NO_3^-. Consequently, the remained powders were maintained at 500 °C for 0.5 h before quenching to room temperature. Finally, the as-prepared sample was washed with distilled water and absolute alcohol for several times and dried at 80 °C. For comparison, bulk $BiFeO_3$ was prepared by traditional solid state method according to Ref. [4].

2.2. Characterization

The phase of the samples were examined by X-ray diffraction (XRD) patterns on a Bruker D8 Advanced diffractometer. The patterns were collected using unfiltered Cu K_α-radiation and the Bragg–Brentano geometry over the 2θ range 10–80°. The morphology of the as-prepared sample was observed by transmission electron microscopy (TEM, Hitachi, Model H-800, accelerating voltage 200 kV). UV–vis absorption spectrum of the sample was obtained on a Shimadzu UV2450 UV–vis spectrophotometer with an integrating sphere.

The equipment for photocatalytic reaction is self-designed. The visible-light source was a 500 W Xe lamp positioned in a quartz cold trap which was in the

* Corresponding author.
E-mail address: xiongwang@mail.njust.edu.cn (X. Wang).

0925-8388/$ – see front matter © 2011 Elsevier B.V. All rights reserved.
doi:10.1016/j.jallcom.2011.03.074

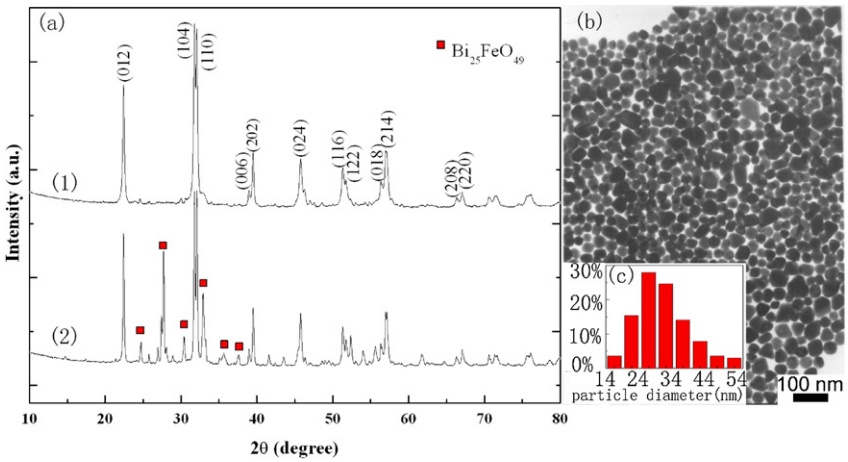

Fig. 1. (a) XRD patterns of the samples calcined at (1) 500 °C and (2) 600 °C, respectively. (b) TEM image and (c) the size distribution (histogram) of the prepared $BiFeO_3$ nanoparticles.

middle of multiposition cylindrical reaction vessel. The system was cooled by wind and water and was maintained at the room temperature. Appropriate cutoff filters were placed around the cold trap to ensure complete removal of radiation below 400 nm and to ensure that the catalysis of the RhB/$BiFeO_3$ system occurred only under visible light.

In the experiment, 0.02 g $BiFeO_3$ was added to 10 mL RhB solution (10^{-5} mol L^{-1}) in the vessel. Before illumination, the suspensions were stirred in the dark for 1 h to ensure the establishment of an adsorption–desorption equilibrium between the photocatalyst and RhB. Then the solution was exposed to visible light irradiation under stirring. At given time intervals, 3 mL suspension was sampled and centrifuged to remove the photocatalyst particles. Then, the UV–vis adsorption spectrum of the centrifugated solution was recorded by a spectrophotometer. Experiments under different pH were also carried on to reveal the role of pH value played on the photocatalytic activity of $BiFeO_3$ nanoparticles. The pH values were adjusted by adding HCl or NaOH. The photocatalytic property of bulk $BiFeO_3$ was also studied for comparison.

3. Results and discussion

Fig. 1(a) shows the XRD patterns of the prepared $BiFeO_3$ samples calcined at different temperatures. All diffraction peaks of the sample prepared at 500 °C can be indexed to rhombohedral $BiFeO_3$ according to the reported data (JCPDS No.71-2494), and the lattice parameters were calculated as $a = b = 5.5774$ Å and $c = 13.8667$ Å. As increasing the calcination temperature to 600 °C, the crystallization of the sample slightly increased, while higher heating temperature induced the formation of the impurity $Bi_{25}FeO_{40}$. The morphology of the pure phase $BiFeO_3$ sample was investigated by TEM. As shown in Fig. 1(b) and (c), it is clear that the particles exhibit an average diameter of about 35 nm with narrow size distribution. The above results confirm that the pure rhombohedral $BiFeO_3$ nanoparticles can be successfully prepared by the sol–gel rapid calcination method with EG as solvent at relatively low temperature.

The high-resolution XPS core spectra of Bi 4f and Fe 2p for the $BiFeO_3$ nanoparticles are presented in Fig. 2. As shown in Fig. 2(a), the peaks at 157.9 and 163.2 eV correspond to the binding energy of Bi $4f_{7/2}$ and $4f_{5/2}$ of Bi^{3+}, respectively. In Fig. 2(b), the binding energy of 710.8 and 724.4 eV correspond to the Fe $2p_{3/2}$ and $2p_{1/2}$ peaks arising from the spin–orbital interaction. No shoulder was observed around the Fe 2p peaks. Moreover, a satellite peak at 718.8 eV was found about 8 eV above the Fe $2p_{3/2}$ peak, which was considered as the characteristic of the oxidation state of Fe [14]. Due to different d orbital electron configurations, Fe^{2+} and Fe^{3+} exhibit a satellite peak at 6 or 8 eV above their $2p_{3/2}$ principal peaks, respectively [15]. No peaks for Fe^{2+} were detected. It can be verified that Fe is in the +3 valence state in the sample. Additionally, the inset of Fig. 2(b) exhibits the symmetrical O 1s core spectrum with binding energy of 531.9 eV, further confirming the single phase of the as-prepared $BiFeO_3$ nanoparticles.

The UV–vis absorption spectrum of $BiFeO_3$ nanoparticles is shown in Fig. 3. A steep absorption edge at about 600 nm was observed due to the band gap absorption. The electronic band at 3.2 eV (388 nm) can be assigned as minority channel dipole-allowed charge transfer excitations and the long tail from 600 to 800 nm is due to the scattering [16–18]. The optical absorption coefficient near the band edge follows the equation $(\alpha h\nu)^n = B(h\nu - E_g)$, where α, h, ν, E_g and B are absorption coefficient, Planck constant, light frequency, band gap, and a constant, respectively. The absorption

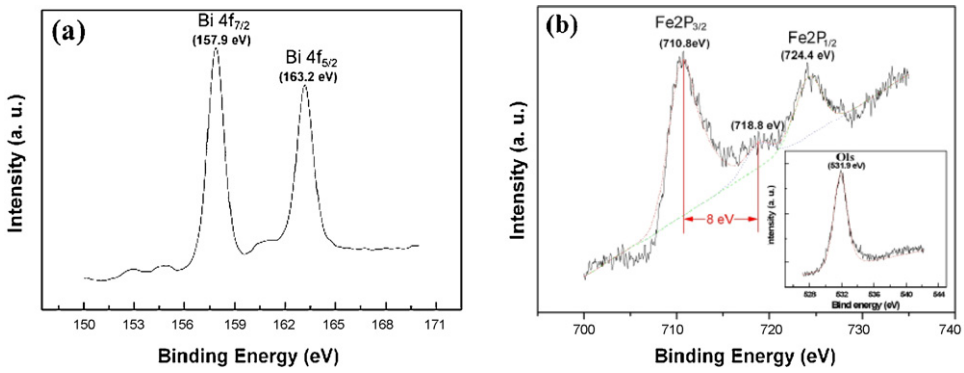

Fig. 2. XPS core spectra of (a) Bi 4f, (b) Fe 2p for the as-synthesized bismuth ferrite nanoparticles. The inset shows the O 1s core spectrum.

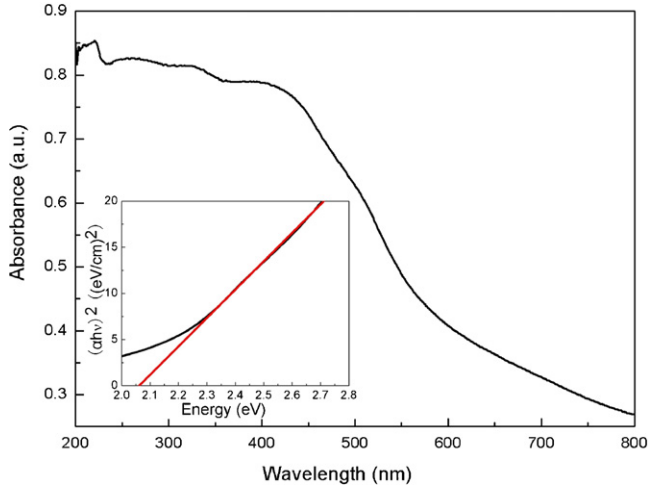

Fig. 3. UV–vis absorption spectrum of the obtained $BiFeO_3$ nanoparticles. The inset shows the corresponding $(\alpha h\nu)^2 \sim h\nu$ plot.

coefficient α was obtained as $\alpha = A/(t \cdot \log e)$, where A is the measured absorbance obtained from the UV–vis spectrum and t is the thickness of the cuvette. The corresponding $(\alpha h\nu)^2 \sim h\nu$ plot for the sample is shown in the inset of Fig. 3. This relationship gives the band gap (E_g) by extrapolating the straight portion of $(\alpha h\nu)^2$ against $h\nu$ plot to the point $\alpha = 0$. Because of the plot of obvious linear nature, the value of n for $BiFeO_3$ is 2, indicating that it is a direct band gap material. The band gap is estimated about 2.06 eV by the linear extrapolation, which is quite comparable with previous results 2.1 eV and 2.03 eV [19,20] and smaller than that of the bulk $BiFeO_3$ (2.8 eV) [21]. Therefore, $BiFeO_3$ nanoparticles may have a potential application as promising photocatalytic decomposition material in the expanded visible-light region.

To determine the photocatalytic activity of the $BiFeO_3$ nanoparticles, the photocatalytic performances were investigated by the degradation of RhB aqueous solution. RhB was selected as the model pollutant because of its obvious absorption at 553 nm. Fig. 4(a) displays the temporal evolution of the spectra during the photodegradation when pH 0.5. The rapid decrease of RhB absorption at the wavelength of 553 nm demonstrated the decomposition of RhB [22] and after only 60 min RhB in the solution was totally decomposed.

Furthermore, the photocatalytic kinetics of the $BiFeO_3$ nanoparticles under different pH values and that of bulk $BiFeO_3$ were also investigated. Langmuir–Hinshelwood model expressed in Eq. (1) was applied to understand the reaction kinetics quantitatively. This model has been used to calculate the rate constant of photocatalytic experiments before [23].

$$r = -\frac{dc}{dt} = \frac{k_r K C}{1 + KC} \tag{1}$$

where r is the reaction rate, k_r is the reaction rate constant, K is the absorption coefficient of the reactant, and C is the reactant concentration. When C is very small, Eq. (1) can be expressed by Eq. (2).

$$r = \frac{-dC}{dt} = k_r K C = kC \tag{2}$$

where k is the first-order rate constant. Set $t = 0$, $C = C_0$, Eq. (3) can be induced.

$$\ln \frac{C_0}{C} = kt \tag{3}$$

Fig. 4(b) shows the photocatalytic activities of $BiFeO_3$ nanoparticles at different pH values (pH 0.5, 2.5, 4.5, 6.5, 8.5, 10.5 and 12.5, respectively), as well bulk $BiFeO_3$. It is clear that the kinetic

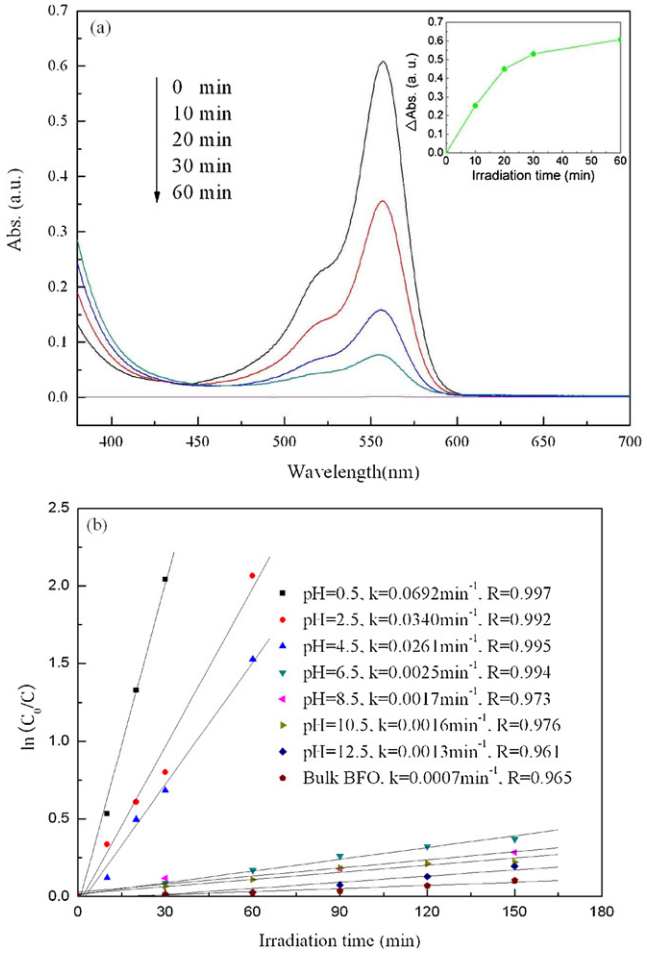

Fig. 4. (a) Absorption changes of RhB solution in visible-light-induced photocatalytic process when pH 0.5. (b) The photocatalytic kinetics of $BiFeO_3$ nanoparticles under different pH values.

simulation curve with irradiation time (t) as abscissa and $\ln(C_0/C)$ as the vertical ordinate is close to a linear curve with the fitting constant R above than 0.96. $BiFeO_3$ nanoparticles have much higher photocatalytic activity than the bulk $BiFeO_3$, which may be due to their large surface area providing more reaction sites. Besides, the scattering effect could not be ignored for the bulk $BiFeO_3$, leading to the reduction of absorption. Obviously, the acidity of the RhB solution remarkably influences the photocatalytic behavior of bismuth ferrite. As for $BiFeO_3$ nanoparticles, the photocatalytic activity markedly improved with decreasing pH values. Because pH value of the solution influences the absorption of the dye molecules on the surface of the catalyst which is very important during photodegradation. When in the acid solution, large amount of positive charges accumulated on the surface of $BiFeO_3$ nanoparticles were benefit for the dispersion of the nanoparticles and the subsequent photochemical reaction. Whereas, when in the alkaline environment, negative charges on the surface of nanoparticles were conducive to the absorption of the positive RhB molecules, leading to the reduction of the active sites for photocatalytic reaction [24]. Moreover, due to their large surface area offering more reaction sites, $BiFeO_3$ nanoparticles exhibit much enhanced photocatalytic activity ($k = 0.0692\ min^{-1}$ at pH 0.5), almost 100 times higher than that of the bulk ($k = 0.0007\ min^{-1}$).

Fig. 5 shows the process of the catalytic reaction and catalyst collection of the $BiFeO_3$ nanoparticles/RhB system. The reddish orange color of the solution disappeared after a total degradation and the turbid solution quickly became clear when an external

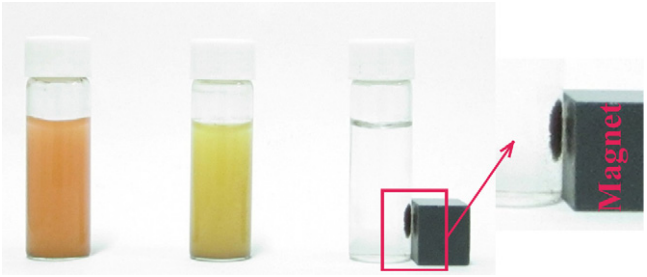

Fig. 5. Photo of the catalytic reaction process and the collection of $BiFeO_3$ nanoparticles.

magnetic field was applied. It suggests that the weak ferromagnetism of $BiFeO_3$ nanoparticles will greatly facilitate the separation and reuse of the catalyst. The combination of weak ferromagnetism and enhanced visible-light-induced photocatalytic activity endows $BiFeO_3$ nanomaterials everlasting interests in water treatment.

4. Conclusion

In conclusion, the pure phase $BiFeO_3$ particles with average particle size of 35 nm are successfully prepared by the sol–gel rapid calcination strategy. It indicates that the rapid calcination is a significant technique in the process of fabricating pure phase $BiFeO_3$ nanoparticles. The visible-light-induced photocatalytic activity was also investigated. $BiFeO_3$ nanoparticles exhibit the weak room-temperature ferromagnetism and their higher photocatalytic activity than the bulk, which predicts their promising application in water treatment.

Acknowledgements

This work was supported by the National Natural Science Foundation of China (Grant No. 21001064, 50902069), the National Natural Science Foundation of Jiangsu Province, China (Grant No. BK201022267), the Specialized Research Fund for the Doctoral Program of Higher Education of China (Grant No. 20103219120045), China Postdoctoral Science Foundation (201003587), the Outstanding Scholars Supporting Program of NUST and the NUST Research Funding (Grant No. 2010ZDJH07, XKF09082).

References

[1] J. Wang, J.B. Neaton, H. Zheng, Science 299 (2003) 1719.
[2] N. Hur, S. Park, P.A. Sharma, J.S. Ahn, S. Guha, Nature 429 (2004) 392.
[3] Y.P. Wang, L. Zhou, M.F. Zhang, X.Y. Chen, J.M. Liu, Appl. Phys. Lett. 84 (2004) 1731.
[4] M.M. Kumar, V.R. Palkar, K. Srinivas, S.V. Suryanarayana, Appl. Phys. Lett. 76 (2000) 2764.
[5] X.M. Lv, J.M. Xie, Y.Z. Song, J.M. Lin, J. Mater. Sci. 42 (2007) 6824.
[6] C. Chen, J.R. Cheng, S.W. Yu, L.J. Che, Z.Y. Meng, J. Cryst. Growth 291 (2006) 135.
[7] S. Li, Y.H. Lin, B.P. Zhang, J. Phys. Chem. C 114 (2010) 2903.
[8] H.R. Liu, X.Z. Wang, J. Sol-Gel Sci. Technol. 47 (2008) 154.
[9] X. Wang, Y. Zhang, Z. Wu, Mater. Lett. 64 (2010) 486.
[10] W. Luo, L.H. Zhu, N. Wang, H.Q. Tang, M.J. Cao, Y.B. She, Environ. Sci. Technol. 44 (2010) 1786.
[11] J.K. Kim, S.S. Kim, W.-J. Kim, Mater. Lett. 59 (2005) 4006.
[12] R. Spinicci, M. Faticanti, P. Marini, S.D. Rossi, P. Porta, J. Mol. Catal. A: Chem. 197 (2003) 147.
[13] F. Gao, X.Y. Chen, K.B. Yin, S. Dong, Z.F. Ren, F. Yuan, T. Yu, Z.G. Zou, J.M. Liu, Adv. Mater. 19 (2007) 2889.
[14] D. Kothari, V.R. Reddy, A. Gupta, D.M. Phase, N. Lakshmi, S.K. Deshpande, A.M. Awasthi, J. Phys.: Condens. Matter 19 (2007) 136202.
[15] C. Wandelt, Surf. Sci. Rep. 2 (1982) 1.
[16] U.A. Joshi, J.S. Jang, P.H. Borse, Appl. Phys. Lett. 92 (2008) 242106.
[17] P. Chen, X.S. Xu, C. Koenigsmann, A.C. Santulli, S.S. Wong, J.L. Musfeldt, Nano Lett. 10 (2010) 4526.
[18] S.R. Basu, L.W. Martin, Y.H. Chu, M. Gajek, R. Ramesh, R.C. Rai, X. Xu, J.L. Musfeldt, Appl. Phys. Lett. 92 (2008) 091905.
[19] Y.N. Huo, Y. Jin, Y. Zhang, J. Mol. Catal. A: Chem. 331 (2010) 15.
[20] R.Q. Guo, L. Fang, W. Dong, J. Phys. Chem. C 114 (2010) 21390.
[21] X.S. Xu, T.V. Brinzari, S. Lee, Y.H. Chu, Phys. Rev. B 79 (2009) 134425.
[22] M. Shang, W.Z. Wang, H.L. Xu, Cryst. Growth Des. 9 (2009) 991.
[23] J.H. Xu, W.Z. Wang, M. Shang, Appl. Catal. B: Environ. 93 (2010) 227.
[24] C.H. Wu, Dyes Pigment 77 (2008) 31.